# Irreversibility line in Nb/CuMn multilayers with a regular array of antidots

C. Attanasio, T. Di Luccio, L. V. Mercaldo, S. L. Prischepa,* R. Russo,† M. Salvato, and L. Maritato
*Dipartimento di Fisica and INFM, Università degli Studi di Salerno, Baronissi (Sa), I-84081, Italy*

S. Barbanera
*IESS-CNR, Via Cineto Romano 42, Roma, I-00100, Italy*

A. Tuissi
*CNR TeMPE, Via Cozzi 53, Milano, I-20125, Italy*
(Received 13 January 2000)

The transport properties of superconducting multilayers with a regular array of antidots obtained by electron-beam lithography have been measured at different temperatures in the presence of external perpendicular magnetic fields. Hysteresis in the $I$-$V$ characteristics was observed, which disappears when approaching the upper critical magnetic field curve $H_{c2}(T)$. By comparing these data with other results (Arrhenius plots of resistive transition curves, $\log V$-$\log I$ characteristics) we have been able to relate the onset of the hysteresis to the presence of an irreversibility line. We discuss several possible mechanisms to clarify the nature of this line. Among them the most plausible seems to be vortex melting mainly induced by quantum fluctuations.

## I. INTRODUCTION

The task of increasing the critical current density $J_c$ in superconducting materials has always been a widely studied subject,[1] gaining even more interest after the discovery of high-temperature superconductors (HTS's).[2] These studies are related to knowledge of the flux-line pinning mechanism and reduction of the vortex mobility. Introducing artificial defects in superconducting materials, such as, for example, nonsuperconducting distributed phases,[3,4] columnar tracks of amorphous material obtained with high-energy ions,[5] or geometrical constrictions such as channels or dots,[6,7] is a very useful tool for better understanding the vortex dynamics and for obtaining higher $J_c$ values. The recent development of submicrometer electron-beam lithographic techniques has made it possible to reduce the typical size of these geometrical constrictions to values much smaller than the period of the vortex lattice, and comparable to typical superconducting coherence lengths.[4,8–10] Many experiments performed on systems with such a regular array of defects,[8–12] and several numerical simulations,[13,14] have been focused on study of the vortex properties at low magnetic fields close to the matching fields $H_n = n_p \Phi_0$ (here $n_p$ is the pins concentration and $\Phi_0$ is the flux quantum).

Other studies, performed at higher magnetic fields, have been related to analysis of the vortex lattice shear stress in superconducting layered systems with artificially obtained weak pinning channels embedded in a strong-pinning environment.[6,7,15,16] Due to the possibility of varying in a controlled way many different parameters, such as the density, the dimensionality, and the nature of the pinning centers,[4,9,17] it is of great interest to study the vortex dynamics in artificially layered conventional superconductors with simultaneous presence of a regular array of pinning centers perpendicular to the layers. Moreover, the natural layered structure of HTS's allows use of these artificial systems as a model to help in discriminating among intrinsic and dimensional effects in the transport properties of HTS compounds.[18]

In this paper we report on current-voltage ($I$-$V$) characteristic and resistance versus temperature $R(T,H)$ measurements in perpendicular external magnetic fields $H$, performed on two different series of Nb/CuMn multilayers with a square array of antidots. The choice of a superconducting (Nb)/spin glass (CuMn) layered system might be interesting particularly in view of its use as a model of HTS compounds. In fact, in many HTS's, the interaction between superconducting and magnetic effects seems to play an important role in determining their peculiar transport properties.[19] Moreover, due to the increased pair-breaking effect in the magnetic layers, decoupling between adjacent superconducting layers can be obtained with a smaller CuMn thickness (when compared, for example, to the case of Nb/Cu multilayers), reaching a situation closer to that observed in HTS's, where the typical distances between superconducting planes are of the order of 10 Å. Finally, as we will see below, a very small spacing between adjacent superconducting layers is crucial in order to enhance the contribution of quantum fluctuations. The two series have antidots with the same diameter $D \approx 1\ \mu$m and different lattice distances between the antidots: $d \approx 2\ \mu$m in one series and $d \approx 1.6\ \mu$m in the other. The experiments were performed on different samples having different anisotropies for each series. The $I$-$V$ curves measured at different temperatures and at different values of $H$ show, in regions of the $H$-$T$ phase diagram depending on the anisotropy of the system, a hysteretic behavior with sudden voltage jumps, which disappears on approaching the critical field $H_{c2}(T)$ curve. From analysis of the curvature of the logarithmic $I$-$V$ characteristics and from study of the shape of the Arrhenius plots of the resistive transition curves, we have been able to relate the disappearance of such hysteresis to the presence of an irreversibility line (IL). We discuss different possible mechanisms responsible for this IL. Among them the most plausible for our samples seems to be

 

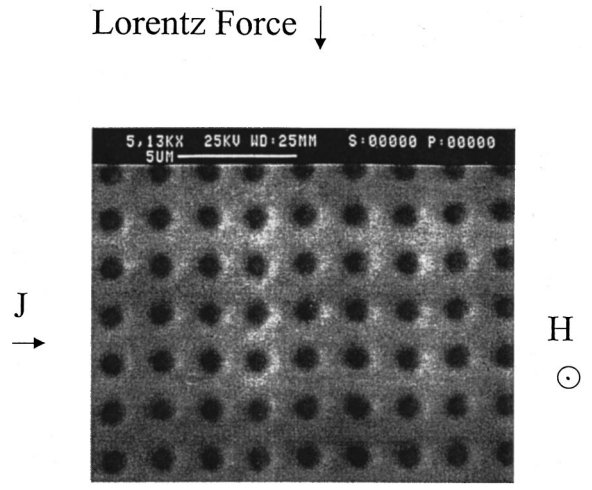


FIG. 1. Scanning electron microscope picture of a Nb/CuMn sample with a square lattice of antidots ($D \approx 1\ \mu$m and $d \approx 2\ \mu$m).

vortex melting mainly induced by quantum fluctuations.[20]

## II. EXPERIMENT

Regular arrays of antidots have been fabricated using electron-beam lithography to pattern the resist on a 2 in. Si(100) wafer. The Nb and CuMn layers were deposited by a dual-source magnetically enhanced dc triode sputtering system with a movable substrate holder onto the patterned resist and the final structures were obtained by the lift-off technique. Single antidots have a circular geometry and the antidot array is arranged in a square lattice configuration (see Fig. 1). The total area covered by the array is a square of $200 \times 200\ \mu\text{m}^2$ with four separate contact pads connected to the vertices. Eight replicas of this structure are present on the same Si wafer to allow the fabrication of a series of multilayered samples with the same Nb thickness and variable CuMn thicknesses in only one deposition run.[21] The resist used is UV III from Shipley; UV III is a chemically amplified photoresist for the deep-UV range, but is widely used as an *e*-beam resist because it provides a good tradeoff between reasonable sensitivity and high resolution. In our case it was used as a positive resist, that is, the resist is retained where unexposed. A resist film thickness of 5800 Å was obtained by spinning the wafer at 1800 rpm. The resist was exposed using a Leica Cambridge system, model EBMF 10, operated at 50 kV. Several tests were carried out in order to achieve structure profiles most suitable for lift-off. In particular, the desired profile is that showing a moderate undercut. Also, developing times and postexposure treatment were optimized for profile improvement. After developing and postbaking at 130 °C the samples underwent reactive ion etching (RIE) in $O_2$ for 30 s at 25 W rf power and 14 Pa oxygen pressure, in order to completely remove residual resist in the exposed areas. This treatment lowered the resist thickness to about 5000 Å. Figure 1 shows a scanning electron microscope image of the typical result of the fabrication process: in this case the antidot nominal diameter is $1\mu$m and the nominal period of the structure is 2 $\mu$m.

The number of bilayers of Nb and CuMn is always equal to six. The first layer is CuMn, the last one is Nb. The Nb nominal thickness $d_{\text{Nb}}$ is 250 Å for all the samples in both the series. The CuMn thickness $d_{\text{CuMn}}$ was varied from 7 to 25 Å in one series ($d \approx 2\ \mu$m) and from 4 to 20 Å in the other ($d \approx 1.6\ \mu$m). The Mn percentage is always equal to 2.7. For reference a Nb/CuMn multilayer with $d_{\text{CuMn}} = 13$ Å (Mn = 2.7 at. %) without antidots, but with the same configuration ($200 \times 200\ \mu\text{m}^2$ square and four pads connected to the vertices), was fabricated. The sample parameters are summarized in Table I. $I$-$V$ characteristics were registered at $T \leqslant 4.2$ K using a dc pulse technique. The temperature stabilization, during the acquisition of curves in the helium bath, was better than $10^{-2}$ K. The magnetic field was obtained with a superconducting Nb-Ti solenoid. From the measured temperature dependencies of the perpendicular and parallel upper critical fields $H_{c2}$ [obtained at half of the resistive transitions $R(T,H)$] we deduced the values for the parallel and perpendicular coherence lengths at zero temperature, $\xi_{\parallel}(0)$ and $\xi_{\perp}(0)$, respectively, and then the value of the anisotropic Ginzburg-Landau mass ratio $\gamma_0 = \xi_{\perp}(0)/\xi_{\parallel}(0)$.[22] The different values of the critical temperatures for samples of the two series having similar values of $d_{\text{Nb}}$ and $d_{\text{CuMn}}$ are probably related to the different Nb quality obtained in the two deposition runs.

Figure 2(a) shows $I$-$V$ curves for sample NCMF at $T = 2.60$ K for different applied magnetic fields in the range $0.03 < H < 0.70$ T. At low magnetic fields the curves present hysteresis, not due to thermal effects, when measured in both forward and backward directions, i.e., by increasing and de-

TABLE I. Some of the relevant sample features. $\rho_N$ is the resistivity at $T = 10$ K. See the text for the meaning of the other quantities.

| Sample | $d_{\text{Nb}}$ (Å) | $d_{\text{CuMn}}$ (Å) | $T_c$ (K) | $\xi_{\parallel}$ (Å) | $\gamma_0$ | $c_L$ | $\rho_N$ ($\mu\Omega$ cm) | Antidot lattice | $G_i$ | $Q^*$ |
|---|---|---|---|---|---|---|---|---|---|---|
| NCMB | 250 | 7 | 3.21 | 97 | 1.0 | 0.31 | 16.5 | yes $d \approx 2\ \mu$m | $2.08 \times 10^{-8}$ | $5.7 \times 10^{-2}$ |
| NCMC | 250 | 10 | 3.20 | 95 | 1.5 | 0.19 | 13.3 | yes $d \approx 2\ \mu$m | $4.26 \times 10^{-8}$ | $3.2 \times 10^{-2}$ |
| NCMD | 250 | 13 | 3.00 | 108 | 2.2 | 0.16 | 11.8 | yes $d \approx 2\ \mu$m | $6.4 \times 10^{-8}$ | $2.2 \times 10^{-2}$ |
| NCMF | 250 | 19 | 3.51 | 113 | 2.3 | 0.10 | 11.8 | yes $d \approx 2\ \mu$m | $8.4 \times 10^{-8}$ | $1.5 \times 10^{-2}$ |
| NCMH | 250 | 25 | 3.76 | 115 | 2.5 | 0.09 | 11.2 | yes $d \approx 2\ \mu$m | $1.17 \times 10^{-7}$ | $1.09 \times 10^{-2}$ |
| RNCMA | 250 | 4 | 6.41 | 82 | 1.5 | 0.27 | 8.6 | yes $d \approx 1.6\ \mu$m | $2.7 \times 10^{-7}$ | $5.22 \times 10^{-2}$ |
| RNCMC | 250 | 12 | 6.01 | 90 | 1.7 | 0.16 | 11.7 | yes $d \approx 1.6\ \mu$m | $2.1 \times 10^{-7}$ | $2.18 \times 10^{-2}$ |
| RNCME | 250 | 20 | 4.65 | 112 | 2.2 | 0.14 | 11.6 | yes $d \approx 1.6\ \mu$m | $1.6 \times 10^{-7}$ | $1.39 \times 10^{-2}$ |
| NCMDA | 250 | 13 | 5.38 | 110 | 2.5 | | 12.6 | no | | |

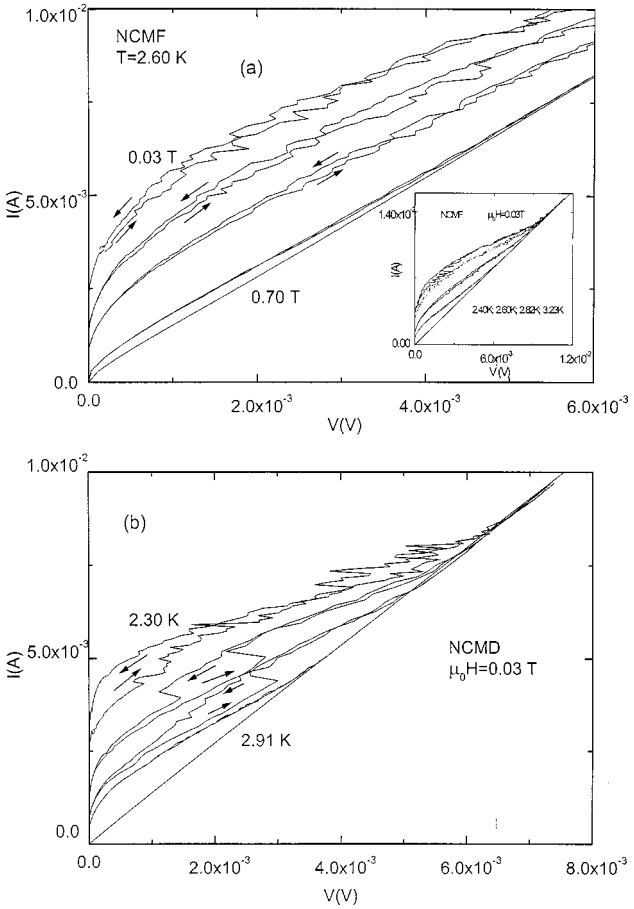


FIG. 2. (a) Current-voltage characteristics for the multilayer NCMF at $T=2.60$ K for different magnetic field values. The increasing values are 0.03, 0.06, 0.15, 0.55, 0.70 T. (b) Current-voltage characteristics for the multilayer NCMD at $H=0.03$ T for different temperatures. The increasing values are 2.30, 2.34, 2.60, 2.80, 2.91 K. In the inset of (a) the $I$-$V$ characteristics of the sample NCMF are shown at $H=0.03$ T for different temperatures. The increasing values are 2.40, 2.60, 2.82, 3.23 K.

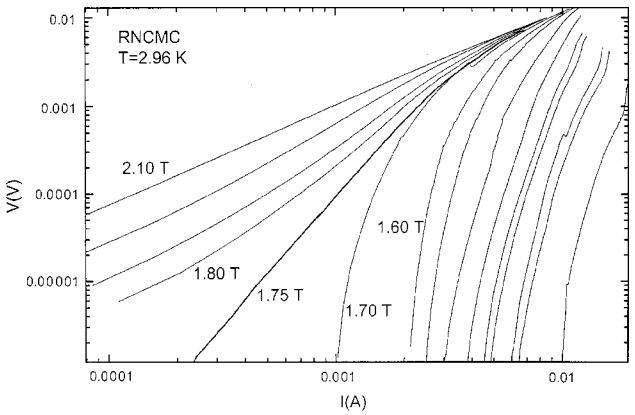


FIG. 3. Logarithmic current-voltage characteristics for the sample RNCMC at $T=2.96$ K for magnetic fields increasing counterclockwise of 0.20, 0.40, 0.50, 0.80, 0.90, 1.10, 1.30, 1.50, 1.60, 1.70, 1.75, 1.80, 1.85, 1.95, 2.10 T. The numbers indicate some values of the magnetic field. The melting field is estimated to be equal to 1.75 T.

creasing the current.[17] Such hysteresis becomes smaller when $H$ is increased, disappearing completely, in the limit of our experimental accuracy, when approaching $H_{c2}$. These features were repeatedly obtained for the same sample in different measurements and are typical for all the samples of the two series with antidots. In Fig. 2(b) the $I$-$V$ characteristics for sample NCMD are plotted in the temperature range $2.30<T<2.91$ K for $\mu_0 H=0.03$ T. In this case the hysteresis disappears on approaching $T_c$. A similar behavior is shown in the inset of Fig. 2(a), where the $I$-$V$ characteristics of sample NCMF are plotted in the temperature range $2.40<T<3.23$ K. The $I$-$V$ curves for sample NCMDA without antidots are always smooth and paraboliclike, typical of a type-II superconductor.

In Fig. 3, we plot the $I$-$V$ curves on a double logarithmic scale for sample RNCMC at $T=2.96$ K for different values of the magnetic field. A change in the curvature of the log $V$-log $I$ curves clearly occurs at low voltages; this is usually related to the presence of an IL in the $H$-$T$ phase diagram,[23] given by the points at which the log $V$-log $I$ curve is linear. In all the samples measured, these points are always very close to the points at which the hysteresis in the $I$-$V$ curves disappears. As an example, in Figs. 4(a)–4(c) are shown the $H$-$T$ phase diagrams for samples NCMB, NCMC, and NCMF, respectively. Circles distinguish the two different regimes of the vortex dynamics as determined from the disappearance of the hysteresis in the $I$-$V$ curves; up triangles indicate points where change in the curvature of the log $V$-log $I$ curve occurs; squares correspond to the values of the perpendicular critical magnetic field. It is evident that the change in the hysteretical behavior of the $I$-$V$ characteristics is related to the IL as defined by the change in the log $V$-log $I$ curvature. It is also interesting to note that the position of the IL in the $H$-$T$ plane moves away from the $H_{c2}$ lines as the anisotropy of the samples increases. We want to point out that in the $H_{c2}(T)$ curves measured in our samples, an upward curvature is always present. This feature has often been observed in many superconducting systems, and can be related to small inhomogeneities present in the samples.[24,25]

Another way to determine the presence of an IL in the $H$-$T$ phase diagram of a superconductor is to study the Arrhenius plot of the resistance versus temperature curves.[18] In particular, it has been shown that IL's defined by studying the Arrhenius plots in the presence of external magnetic fields coincide with those obtained using a criterion of equality between the ac (120 Hz) measured resistivity $\rho_{\mathrm{ac}}$, and the flux-flow resistivity $\rho_{\mathrm{FF}}$ measured from $I$-$V$ characteristics.[26,27] In Fig. 5 the Arrhenius plot of the transiton curves, recorded using a bias current of 2 mA, of sample RNCMA is shown at different perpendicular magnetic fields. A well-defined field-dependent temperature $T^*$ separates two zones with very different activation energies. In particular, at $T<T^*$ a sudden increase in the Arrhenius slope signals a transition in the transport properties of the sample that can be related to the presence of the IL. In Fig. 6 is shown the measured $H$-$T$ phase diagram for sample RNCMC. The solid squares correspond to perpendicular magnetic fields; the open squares correspond to the points in the $H$-$T$ plane at which the onset of hysteresis in the $I$-$V$ curves takes place; the open diamonds are defined taking into account the change of curvature of the log $I$-log $V$ curves; and the open circles and up triangles are the points at which the slope

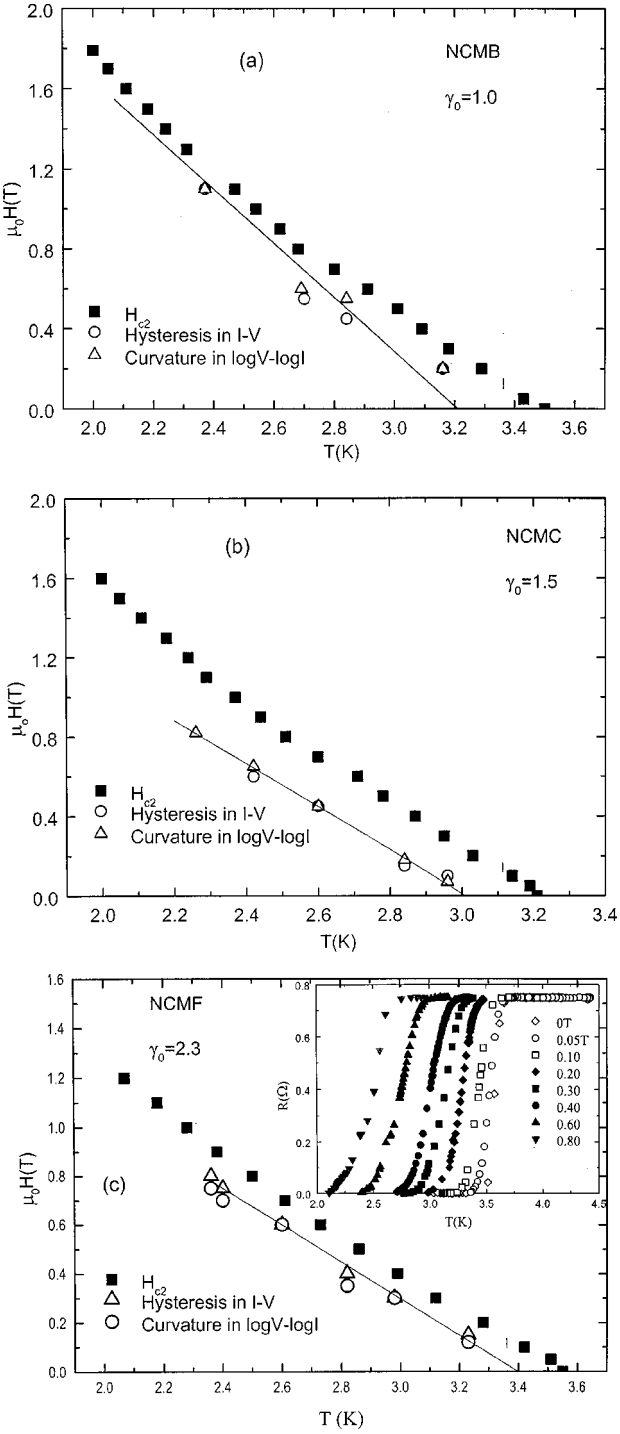


FIG. 4. *H-T* phase diagram for sample (a) NCMB, (b) NCMC, and (c) NCMF. Squares correspond to $H_{c2\perp}$, circles correspond to the disappearance of hysteresis in the *I-V* curves, up triangles correspond to the change of curvature in the log *V*-log *I* curves. The solid lines are calculated according to Eq. (3). In the inset of (c) are shown the transition curves at different magnetic fields for sample NCMF.

in the Arrhenius plot of the transition curves, taken, respectively, at a bias current of 2 and 6 mA, change as seen in Fig. 5. It is evident that in this case also all the points (open symbols) fall again on the same curve, which can be identified as an II.

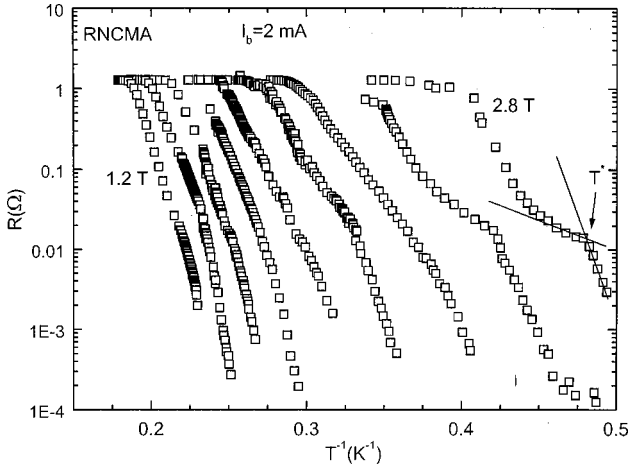


FIG. 5. Arrhenius plot of the transition curves for sample RNCMA in perpendicular magnetic fields. The increasing magnetic field values are 1.2, 1.4, 1.6, 1.8, 2.0, 2.2, 2.4, 2.6, 2.8 T. The numbers indicate some values of the magnetic field. The curves were recorded using a bias current $I_b = 2$ mA.

### III. DISCUSSION

In all the measurements performed the bias current was applied in the plane of the film and perpendicular to the direction of the external magnetic field (see Fig. 1). In this configuration, the Lorentz force acting on the vortices tends to move them along the channels between the antidots. On the other hand, in the narrower zones between adjacent antidots, the current density is much higher than in the channels, so that we locally have weaker pinning centers in these parts of the sample. Therefore, we can look at our superconducting layered system as made of alternating zones of strong pinning (the channels along the direction of action of the Lorentz force in Fig. 1) and weak pinning (the narrower zones between adjacent antidots), like other cases reported in the literature.[6,7,15,16] The value of the matching field in both the series is very small, $H_n \approx 5$ Oe, and also $d \gg \xi(T)$, where $\xi(T)$ is the temperature-dependent coherence length, which in our multilayers has typical values of about 100 Å. There-

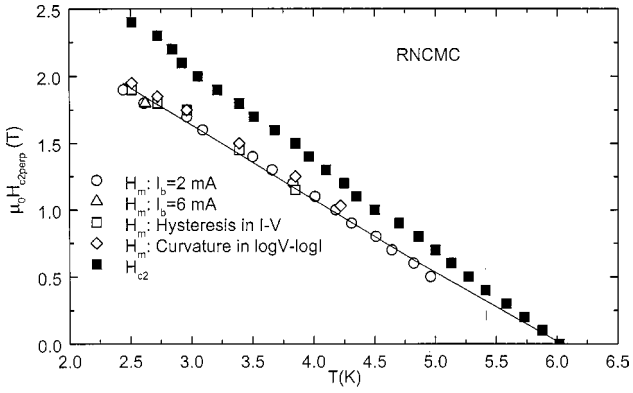


FIG. 6. *H-T* phase diagram for sample RNCMC. Solid squares correspond to $H_{c2\perp}$, open squares correspond to the disappearance of hysteresis in the *I-V* curves, diamonds correspond to the change of the curvature in the log *V*-log *I* curves, circles (up triangles) correspond to the $T^*(H)$ values extracted from the Arrhenius plot using a bias current of 2(6) mA. The solid line has been calculated according to Eq. (3).

fore, in the superconducting state it is possible to have a vortex lattice inside the channels between the antidots. The pinning of these interstitial vortices is determined mostly by the intrinsic properties of the superconducting materials.[10,28]

To start the analysis of our data we have first to determine the dimensionality of the vortex lattice in our samples. At magnetic fields lower than a critical value $H_{cr} \approx 4\Phi_0/\gamma_0^2 s^2$, where $s$ is the interlayer distance between superconducting layers, the vortices in adjacent layers are strongly coupled and vortex lines behave as if three dimensional (3D). For our samples $H_{cr} \approx 10^3$ T, well above any applied fields, and we can exclude the appearance of decoupling of the vortex lines in our layered systems.[29]

On the other hand, when the shear modulus $c_{66}$ of a vortex lattice is much lower than the tilt modulus $c_{44}$, the system can behave bidimensionally. In principle, thermal fluctuations could cause tilt deformations in the vortex line. The critical thickness value $d_{cr}$ of a film beyond which thermal-fluctuation-induced tilt deformations become relevant is given by[30]

$$d_{cr} \approx \frac{4.4\xi_{\parallel}}{\sqrt{h(1-h)}}, \tag{1}$$

where $h = H/H_{c2}$. In multilayers, however, the $d_{cr}$ value is reduced by a factor $\gamma_0^2$,[29] which for our samples gives, in the range of measured temperatures and magnetic fields, $d_{cr}^{multi} \approx 200-300$ Å. Typical thicknesses for our samples are in the range 1500–1700 Å. This means that the vortex lattice in our multilayers is in a strongly 3D regime.

One of the proposed interpretations of the nature of the IL relies upon a depinning mechanism in which a crossover from flux creep to flux flow occurs.[31] In our samples we never obtain linearity of the $I$-$V$ curves either at high voltage, where a uniform flux flow should be present, or at small currents, where thermally assisted flux flow[32] should take place. If we fit our data with the relation $V \sim I^{\alpha}$ the fitting exponent is always very high ($\alpha > 10$). Therefore we exclude the possibility of flux-creep–flux-flow crossover in the presence of a pinning strength distribution that could also be responsible for the curvature change of the $I$-$V$ curves when plotted in double logarithmic scale.[33]

The $I$-$V$ curves shown in Figs. 2(a) and 2(b) are very similar to those obtained as a result of numerical simulations for a superconductor with periodic pinning close to the matching field.[13,14] Considering that we are very far from $H_n$ we cannot apply the results of Ref. 13 to explain our $I$-$V$ curves. Nevertheless, the main observed features indicate the presence of a region in the $H$-$T$ plane where plastic vortex motion probably takes place. Below some crossover value $H_{pl}$, vortices experience plastic motion which usually reveals in hysteresis curves.[34] Above $H_{pl}$, $I$-$V$ curves are smooth, hysteresis vanishes, and the vortex motion starts to be a flow of vortex liquid.[34] The presence of vortex melting below $H_{c2}$ in the $H$-$T$ phase diagram of Nb and Nb-based systems has already been proposed.[26,35,36] While in the case of Nb single crystals and films, the flux lattice transition seems to occur very close to $H_{c2}$,[35,37] in Nb-based multilayers, the anisotropy can substantially lower the melting line.[26,38,39] The vortex melting scenario along with the simultaneous presence of weak- and strong-pinning channels can also explain the observed Arrhenius plots. In fact, immediately below $T_c^{onset}$ (defined as the temperature where the electrical resistance $R$ is 0.9 of its value in the normal state), the solidification of the vortices in the strong-pinning channels determines the high values of the initial slope in the plots. At lower temperatures, the dissipation in the system is mainly due to the vortices in the weak-pinning regions, and this results in a lower value of the activation energies. When these vortices experience the transition from liquid to solid at $T = T^*$, the slope in the plots increases again.[16]

Melting in the vortex lattice can be induced by thermal fluctuations.[38] The melting temperature at which the vortex lattice goes from a solid phase to a liquid one can be obtained by using the 3D thermal melting criterion[38]

$$c_L^4 \approx \frac{3G_i}{\pi^2}\frac{h}{(1-h)^3}\frac{t_m^2}{(1-t_m)}, \tag{2}$$

where $c_L$ is the Lindemann number, $T_c$ is the superconducting transition temperature (defined in our case as the point where the electrical resistance $R$ of the sample becomes less than $10^{-4}\,\Omega$), $t_m = T_m/T_c$ is the reduced melting temperature, and $G_i$ is the Ginzburg number, which determines the contribution of the thermal fluctuations to the vortex melting, given by $G_i = (1/2)[2\pi\mu_0 k_B T_c \lambda_{\parallel}(0)\gamma_0/\Phi_0^2\xi_{\parallel}(0)]$, where $\lambda_{\parallel}$ is the in-plane penetration depth which, for all our samples, has been assumed to be equal to 1500 Å.[40] Melting usually occurs when $c_L \approx 0.1-0.3$.[20] When we try to fit the IL observed in our samples with Eq. (2) we get $c_L \sim 10^{-4}$. This extremely low value for the Lindemann number makes it unreasonable to consider the IL as due to 3D thermal melting.

However, as first pointed out by Blatter and Ivlev,[20] in moderately anisotropic superconductors at low temperatures one cannot exclude the contribution of quantum fluctuations to the melting. In this case the total fluctuation displacement of the vortex line is $\langle u\rangle^2 = \langle u\rangle_{th}^2 + \langle u\rangle_q^2$, where $\langle u\rangle_{th}$ is the average displacement due to thermal fluctuations and $\langle u\rangle_q$ is the average displacement due to quantum fluctuations. $\langle u\rangle_{th}^2$ diminishes with temperature, while $\langle u\rangle_q^2$ does not depend on the temperature and at low values of $T$ one could expect $\langle u\rangle_{th}^2 \leqslant \langle u\rangle_q^2$. The amplitude of $\langle u\rangle_q^2$ depends on the ratio $Q^*/\sqrt{G_i}$ where $Q^* = e^2\rho_N/\hbar s$, with $\hbar$ the Planck constant and $e$ the elementary charge. If $Q^*/\sqrt{G_i} \gg 1$, the contribution of quantum fluctuations is crucial. Obviously, the shorter $s$ is the higher $Q^*$ is. In the case of our samples $s$ goes from 4 to 25 Å while $\gamma$ varies in the range 1 to 2.5. In the case of nonmagnetic spacers, such as, for example, Nb/Cu multilayers, values of $\gamma$ around 2.5 with Nb thickness of 250 Å imply Cu thickness of the order of hundreds of angstroms,[41] therefore strongly reducing $Q^*$.

For the samples discussed here we always get $Q^*/\sqrt{G_i} > 30$ which justifies the possibility of an important contribution coming from quantum fluctuations.[42] In this case the melting line is given by[43]

$$h_m = \frac{4\Theta^2}{\{1+[1+4Q\Theta/t]^{1/2}\}^2} \tag{3}$$

where $h_m = H_m/H_{c2}$, $t = T/T_c$ is the reduced temperature, $\Theta = \pi c_L^2(t^{-1}-1)/\sqrt{G_i}$, $Q = Q^*\Omega\tau/\pi\sqrt{G_i}$, with $\Omega$ a cutoff

frequency generally of the order of the Debye frequency and $\tau$ an effective electronic relaxation time ($\hbar/k_B T_c \approx \tau$).[43] As we already showed,[44] the values of $\Omega$ and $\tau$ in Nb/CuMn are in the range $(2-3)\times 10^{13}$ s$^{-1}$ and $(1-5)\times 10^{-13}$ s, respectively. Therefore, for all the samples studied we have assumed $\Omega = 3\times 10^{13}$ s$^{-1}$ and $\tau = 5\times 10^{-13}$ s. In this way we reduce the number of free fit parameters in Eq. (3) to only one, namely, the Lindemann number $c_L$.

The solid line in Fig. 6 was calculated according to Eq. (3) using for the Lindemann number a value of $c_L = 0.23$. The solid lines in Figs. 4(a)–4(c) have also been calculated according to Eq. (3). For sample NCMC, Fig. 4(b), we obtain good agreement with the experimental data for $c_L = 0.19$, while for sample NCMH, Fig. 4(c), the solid line is obtained by taking $c_L = 0.09$. The agreement between experimental data and theoretical curves is very good for all the samples studied. The $c_L$ values, as shown in Table I, become smaller with increasing anisotropy, reaching in the case of sample NCMH a value slightly below 0.1.[20] When increasing the anisotropy of the system, the coupling between adjacent superconducting layers reduces and vortex lines become softer. The influence of the thermal fluctuations on the vortex dynamics is strongly dependent on this coupling. Qualitatively, therefore, the reduction of the $c_L$ values with increasing anisotropy could be related to the change in the topology of the vortex system.

On the other hand, the softening of the vortex system could also determine a situation in which thermal fluctuations are able to cause tilt deformations. Anyway, if we try to fit the experimental points in Figs. 4 and 6 using the 2D pure thermal melting curve[45]

$$\frac{\alpha d}{\kappa^2}\frac{H_{c2}(T)}{T(1.25-0.25t)}(1-0.58h_m-0.29h_m^2)(1-h_m)^2=1, \tag{4}$$

we do not obtain any agreement with the data. Here $\alpha = A\Phi_0(1.07)^2/32\pi\mu_0 k_B$, $\kappa = \lambda_\parallel/\xi_\parallel$, and $d$ is the thickness of the sample. $A$ is a renormalization factor of the shear modulus $c_{66}$ due to nonlinear lattice vibrations and vortex lattice defects and is $A \approx 0.64$.[46]

We want to point out that the quantum melting theory has been succesfully applied to describe the vortex behavior in unperforated Nb/CuMn multilayers also.[44] In that case the melting line was determined by analyzing in Arrhenius fashion the measured $R(T)$ curves in perpendicular magnetic fields. The shapes of the Arrhenius plots (see, for example, Fig. 1 in Ref. 44) were very similar to those observed in the case of perforated samples, suggesting the presence of two types of pinning centers also in the case of nonperforated samples. In non perforated samples, edge pinning could be relevant and obviously stronger than intrinsic pinning.[47] Therefore one could interpret the shape of the Arrhenius plots in unperforated Nb/CuMn multilayers as due to the vortex transition from liquid to solid, first of the vortices at the edges and then, at lower temperatures, of the vortices intrinsically pinned in the inner part of the sample. If this interpretation is correct, the slopes of the Arrhenius plots measured in unperforated samples in zone 2 (see inset in Fig. 7) should be very close to the slope measured in zone 1 in perforated samples. In fact, in both cases, this slope should

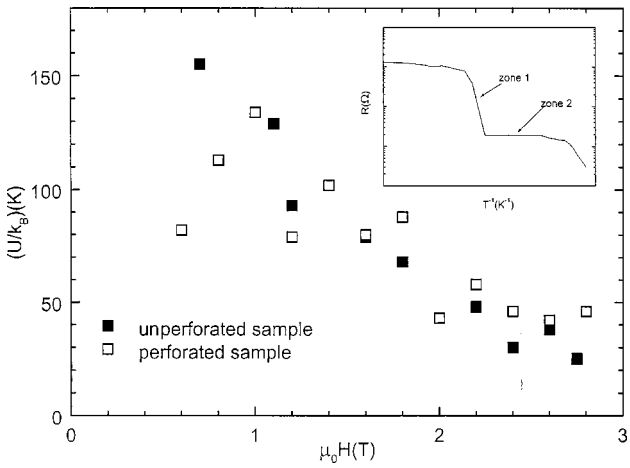


FIG. 7. Values of the activation energy in zone 2 for an unperforated sample (solid squares) and values of the activation energy in zone 1 for a perforated sample (open squares). Inset: Schematic of a typical Arrhenius plot observed in a perforated and an unperforated Nb/CuMn multilayer together with the identification of zones 1 and 2.

be related to the activation energy of vortices intrinsically pinned inside the system. In Fig. 7 the solid points refer to the values of the activation energy in a typical unperforated sample measured in zone 2, while the open symbols refer to the values of the activation energy in a perforated sample (RNCMA) measured in zone 1. The two samples have been chosen to have similar critical temperatures. Also the $R(T,H)$ curves have been taken using a similar value for the bias current density $J_b$. The quite nice agreement between the two sets of data supports our idea that, in both cases, they are a measure of the intrinsic pinning in the material.

The presence of the antidot array in the multilayers makes the vortex melting more easily measurable. In fact, in the case of perforated samples one is able to detect the change in the slope of the Arrhenius plots using low values of the bias current ($\sim$100 $\mu$A) while for unperforated samples bias currents of $\sim$1 nA are needed to observe the same effect (the IL in a superconductor does not depend on the value of the bias current). This is consistent with the idea that in antidotted samples the melting takes place in the zones with weaker pinning when compared to the case of unperforated samples, in which the measured vortex phase transition takes place in the zones of intrinsic pinning. As a consequence of this the hysteresis is also much more easily detectable in antidotted samples, in regions of the $I$-$V$ characteristic not too close to the $H_{c2}(T)$ curve.

The influence of the regular array of antidots on the vortex properties is also confirmed by the behavior in our samples of the vortex correlation length in the liquid phase, $\xi_+$, defined as[48]

$$\xi_+ \approx \xi_{+0}\exp\left\{b\left(\frac{T_m}{T-T_m}\right)^\nu\right\}, \tag{5}$$

where $b$ is a constant of the order of unity, $\nu = 0.369\,63$, and $\xi_{+0}$, being the smallest characteristic length scale in the liquid, is of the order of $a_0$, the vortex lattice parameter. According to the melting theory the shear viscosity $\eta(T)$ of the vortex liquid starts to increase approaching the liquid-solid

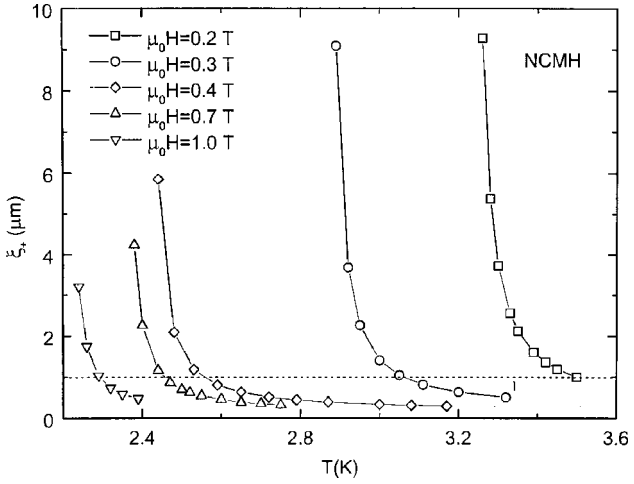


FIG. 8. Dependence of the correlation length $\xi_+$ on temperature at different magnetic fields for sample NCMH.

line from above, when $\eta \sim \xi_+^2(T)$.[48] The curves of $\xi_+$ versus the temperature obtained from Eq. (5) for different applied magnetic fields are reported in Fig. 8 for sample NCMH. All the curves start to diverge when the value of $\xi_+$ becomes of the order of magnitude of the distance between adjacent antidots, i.e., when $\xi_+ \approx d = 1\ \mu$m. Similar results were obtained for all the samples investigated. This is exactly what we expect, if we look at the investigated system as a vortex ensemble constrained in narrow channels among the lines of antidots. In this case, in fact, the melting transition at $H = H_m$ is going to be observed when the correlation length of the liquid $\xi_+$ reaches the value of the width of the channels. The results shown in Fig. 8 clearly indicate the influence of the antidot lattice on the vortex dynamics in our samples.

In conclusion, we have studied transport properties of superconducting (Nb)–spin glass (CuMn) multilayers with a regular array of antidots by measuring $I$-$V$ curves in perpendicular magnetic fields. The measurements were performed far above the matching conditions. The dynamic phase diagram was drawn from analysis of these measurements. Two regions corresponding to plastic flux-flow motion and to motion of the vortex liquid were distinguished. Several interpretations of this effect were considered. Among them, the most plausible seems to be the occurrence of melting mostly due to quantum fluctuations. The presence of the antidots makes it easier to detect the melting, probably because of the presence of weaker pinning in the zones with higher local current density.

*Permanent address: State University of Informatics and RadioElectronics, P. Brovka street 6, 220600, Minsk, Belarus.
†Present address: Dipartimento di Fisica, Università di Roma Tor Vergata, I-00133, Roma, Italy.

[1] A. M. Campbell and J. E. Evetts, Adv. Phys. **21**, 199 (1972).
[2] G. Blatter, M. V. Feigelman, V. B. Geshkenbein, A. I. Larkin, and V. M. Vinokur, Rev. Mod. Phys. **66**, 1125 (1994).
[3] K. Tachikawa, Y. Kuroda, H. Tomori, and M. Ueda, IEEE Trans. Appl. Supercond. **7**, 1355 (1997).
[4] J. J. Martin, M. Vélez, J. Nogués, and I. K. Schuller, Phys. Rev. Lett. **79**, 1929 (1997).
[5] L. Civale, A. Marwick, T. K. Worthington, M. A. Kirk, J. R. Thompson, L. Krusin-Elbaum, Y. Sun, J. R. Clem, and F. Holtzberg, Phys. Rev. Lett. **67**, 648 (1991).
[6] A. Pruijmboom, P. H. Kes, E. van der Drift, and S. Radelaar, Phys. Rev. Lett. **60**, 1430 (1988).
[7] W. K. Kwok, J. A. Fendrich, V. M. Vinokur, A. E. Koshelev, and G. W. Crabtree, Phys. Rev. Lett. **76**, 4596 (1996).
[8] M. Baert, V. V. Metlushko, R. Jonckheere, V. V. Moshchalkov, and Y. Bruynseraede, Phys. Rev. Lett. **74**, 3269 (1995).
[9] D. J. Morgan and J. B. Ketterson, Phys. Rev. Lett. **80**, 3614 (1998).
[10] A. Castellanos, R. Wördenweber, G. Ockenfuss, A. v. d. Hart, and K. Keck, Appl. Phys. Lett. **71**, 962 (1997).
[11] A. T. Fiory, A. F. Hebard, and S. Somekh, Appl. Phys. Lett. **32**, 73 (1978).
[12] A. N. Lykov, Solid State Commun. **86**, 531 (1993).
[13] C. Reichhardt, C. J. Olson, and F. Nori, Phys. Rev. Lett. **78**, 2648 (1997).
[14] C. Reichhardt, C. J. Olson, and F. Nori, Phys. Rev. B **58**, 6534 (1998).
[15] M. H. Theunissen, E. Van der Drift, and P. H. Kes, Phys. Rev. Lett. **77**, 159 (1996).
[16] H. Pastoriza and P. H. Kes, Phys. Rev. Lett. **75**, 3525 (1995).
[17] C. Attanasio, T. Di Luccio, L. V. Mercaldo, S. L. Prischepa, R. Russo, M. Salvato, L. Maritato, and S. Barbanera, Philos. Mag. B **80**, 875 (2000).
[18] W. R. White, A. Kapitulnik, and M. R. Beasley, Phys. Rev. Lett. **66**, 2826 (1991).
[19] A. J. Millis and H. Monien, Phys. Rev. Lett. **70**, 2810 (1995).
[20] G. Blatter and B. I. Ivlev, Phys. Rev. Lett. **70**, 2621 (1993).
[21] L. V. Mercaldo, C. Attanasio, C. Coccorese, L. Maritato, S. L. Prischepa, and M. Salvato, Phys. Rev. B **53**, 14 040 (1996).
[22] M. Tinkham, *Introduction to Superconductivity* (McGraw-Hill, New York, 1996).
[23] P. Berghuis, A. L. F. van der Slot, and P. H. Kes, Phys. Rev. Lett. **65**, 2583 (1990).
[24] V. M. Gvozdikov, Fiz. Nizk. Temp. **25**, 1251 (1999) [Low Temp. Phys. **25**, 936 (1999)].
[25] C. Attanasio, S. Barbanera, T. Di Luccio, S. L. Prischepa, R. Russo, M. Salvato, and L. Maritato, Physica B **284-288**, 618 (2000).
[26] P. Koorevaar, P. H. Kes, A. E. Koshelev, and J. Aarts, Phys. Rev. Lett. **72**, 3250 (1994).
[27] P. Berghuis and P. H. Kes, Phys. Rev. B **47**, 262 (1994).
[28] M. Baert, V. V. Metlushko, R. Jonckheere, V. V. Moshchalkov, and Y. Bruynseraede, Europhys. Lett. **29**, 157 (1995).
[29] L. I. Glazman and A. E. Koshelev, Phys. Rev. B **43**, 2835 (1991).
[30] V. H. Vinokur, P. H. Kes, and A. E. Koshelev, Physica C **169**, 29 (1990).
[31] T. Matsushita and T. Kiss, Physica C **315**, 12 (1999).
[32] P. H. Kes, J. Aarts, J. van den Berg, C. J. van der Beek, and J. A. Mydosh, Supercond. Sci. Technol. **1**, 242 (1989).
[33] A. N. Lykov, C. Attanasio, L. Maritato, and S. L. Prischepa, Supercond. Sci. Technol. **10**, 119 (1997).
[34] M. J. Higgings and S. Bhattacharya, Physica C **257**, 232 (1996).
[35] M. F. Schmidt, N. E. Israeloff, and A. M. Goldman, Phys. Rev. Lett. **70**, 2162 (1993).
[36] J. W. Lynn, N. Rosov, T. E. Grigereit, H. Zhang, and T. W. Clinton, Phys. Rev. Lett. **72**, 3413 (1994).

[37] P. L. Gammel, U. Yaron, A. P. Ramirez, D. J. Bishop, A. M. Chang, R. Ruel, L. N. Pfeiffer, E. Bucher, G. D'Anna, D. A. Huse, K. Mortensen, M. R. Eskildsen, and P. H. Kes, Phys. Rev. Lett. **80**, 833 (1998).
[38] A. Houghton, R. A. Pelcovits, and A. Sudbø, Phys. Rev. B **40**, 6763 (1989).
[39] E. E. Brandt, Phys. Rev. Lett. **63**, 1106 (1989).
[40] L. V. Mercaldo, S. M. Anlage, and L. Maritato, Phys. Rev. B **59**, 4455 (1999).
[41] C. S. L. Chun, G. G. Zheng, J. L. Vicent, and I. K. Schuller, Phys. Rev. B **29**, 4915 (1984).
[42] G. Blatter, B. I. Ivlev, Yu. Kagan, M. H. Theunissen, Y. Volokitin, and P. H. Kes, Phys. Rev. B **50**, 13 013 (1994).
[43] G. Blatter and B. I. Ivlev, J. Low Temp. Phys. **95**, 365 (1994).
[44] C. Attanasio, C. Coccorese, L. Maritato, S. L. Prischepa, M. Salvato, B. Engel, and C. M. Falco, Phys. Rev. B **53**, 1087 (1996).
[45] P. Koorevaar, Ph.D. thesis, Leiden University, 1994.
[46] S. W. de Leeuw and J. W. Perram, Physica A **113**, 546 (1982).
[47] C. P. Bean and J. D. Livingston, Phys. Rev. Lett. **12**, 14 (1964).
[48] D. R. Nelson and B. I. Halperin, Phys. Rev. B **19**, 2457 (1979).